FILAMENTARY GALAXY CLUSTERING: A MAPPING ALGORITHM

J. E. MOODY[1]

Department of Physics, Princeton University

AND

EDWIN L. TURNER[2] AND J. RICHARD GOTT III

Princeton University Observatory

ABSTRACT

The Shane-Wirtanen galaxy count catalog gives the strong visual impression of large-scale linear or filamentary features in the galaxy distribution. Computer simulations of hierarchical galaxy clustering constructed to have two-, three-, and four-point autocorrelation functions like those observed do not have such an appearance. A simple and well-defined algorithm which maps and quantifies filamentary structure is developed. It appears to be successful in identifying those (and only those) filaments which the eye picks out in the Shane-Wirtanen catalog and thus provides an objective tool for studying these structures. A catalog and map of the most prominent Shane-Wirtanen filaments is given. Application of the algorithm to a computer simulation of hierarchical galaxy clustering reveals a set of visually less conspicuous filaments with statistical properties strikingly similar to those of the Shane-Wirtanen filaments in many respects. Long ($\gtrsim 10°$) filaments do occur significantly more frequently in the data than in the simulations and the real filaments do occur at slightly higher relative contrast than the simulation filaments. These facts may explain their greater visual impact. It is not yet clear whether the Shane-Wirtanen filaments can be understood in terms of simple hierarchical galaxy clustering models.

Subject headings: cosmology — galaxies: clustering — numerical methods

I. INTRODUCTION

Maps (Seldner *et al.* 1977) of the Shane-Wirtanen catalog of galaxy counts give most viewers the impression of containing linear or filamentary structures. The most striking of these structures appear to have lengths $\gtrsim 10°$ and widths of $<1°$ as the reader may judge from Figure 1 (Plate 1). The nature of these filaments is not known; they could be real structures in the galaxy distribution with sizes $\lesssim 100\,h^{-1}$ Mpc, the results of patchy galactic obscuration (see Seldner and Uson 1983), statistical fluctuations in an isotropic but clustered galaxy distribution, optical illusions, or artifacts of some unsuspected systematic error in the Shane-Wirtanen counts. If the first of these possibilities is correct, they are probably very important clues to the origin of large-scale structure in the universe and surely merit careful observational study. In this paper we will present a simple and objective algorithm which can be used to map and measure filamentary structures. It is applied to the Shane-Wirtanen map, a randomly scrambled map, and a static computer simulation (Fig. 1) of hierarchical galaxy clustering (Soneira and Peebles 1978) which reproduces the observed $n \leq$ four-point auto-correlation functions.

Before proceeding it is well to note that very large-scale planar or even linear structures in the galaxy distribution are expected theoretically in the Zel'dovich "pancake" model for the evolution of primordial adiabatic perturbations (Zel'dovich, Einasto, and Shandarian 1982; Bond, Efstathiou, and Silk 1980; Doroshkevich *et al.* 1980; Sunyaev and Zel'dovich 1972; Zel'dovich 1970). They might also be explicable in the blast wave galaxy formation theory (Ostriker and Cowie 1981; Ikeuchi 1981). Furthermore, numerous authors (Tully 1982; Davis *et al.* 1982; Gregory, Thompson, and Tifft 1981; Einasto, Joveer, and Saar 1980; Tarenghi *et al.* 1979, 1980; Joveer, Einasto, and Tago 1978; Chincarini 1978; and references therein) believe that they have encountered just such structures in the distribution of galaxies in various deep redshift surveys. Recently Kuhn and Uson (1982) have reported statistical evidence for excess filamentary structure in the Shane-Wirtanen data.

There is also some evidence against the reality of the Shane-Wirtanen filaments in that the three- and four-point galaxy autocorrelation functions show no enhanced amplitudes for shape parameters corresponding to elongated triangles and quadrilaterals (Peebles and Groth 1975; Fry and Peebles 1978). We are not inclined to take this evidence too seriously because these higher order autocorrelation functions drop so rapidly in amplitude relative to the two-point function and are so soon lost in the measurement noise that they are probably insensitive to filamentary clustering.

Finally, it may seem unnecessary to identify and measure filaments by a laborious algorithm when they are so readily apparent to the eye. There is some

---

justification for this view. The eye can readily detect real but subtle patterns which are very difficult to measure using simple statistics. On the other hand, the eye has very low standards of statistical significance for the detection of such signals, presumably due to natural selection. (It is better to flee a perceived but illusory tiger in the bushes than to occasionally not notice a real one.) The primary goal of this paper is to devise a simple, objective algorithm which is sensitive to the same filamentary features picked out by the eye; this may be regarded as a necessary first step toward assessing their reality.

In the next section we describe a simple algorithm for identifying filament ridge lines. In § III this algorithm is applied to the Shane-Wirtanen data and to the control maps; similarities and differences are noted. Section IV contains a catalog of a selected subsample of the Shane-Wirtanen filaments identified by our algorithm. Finally, results and conclusions are discussed in § V.

II. AN ALGORITHM

a) Difficulties and Constraints

It is relatively easy to invent statistics which measure linearity or connectedness in the galaxy clustering distribution; however, extensive analysis and experimentation has taught us that many such simple statistics are unsuitable for a variety of reasons some of which are enumerated below:

1. Some otherwise useful statistics do not count each galaxy equally but rather each pair, triple, quadruple, etc. This is undesirable because it masks any signal from lower density (richness) regions which could have systematically different structure. The n-point autocorrelation functions suffer from this defect.

2. Many obvious statistics essentially ask if there is a significant excess of galaxies in a direction 180° away from another excess direction, as averaged over points in the image. These measures of filamentariness are usually diluted by a negative signal from gradients in the galaxy counts.

3. Many possible filament statistics consist of a number or function which does not explicitly and unambiguously refer to particular structures in the image. For our purposes, such measures are difficult to interpret since it is generally impossible to say if they are referring to the same features which one sees. The self-avoiding random walk analysis of Kuhn and Uson (1982) has this problem.

4. There is a final possible property of a filament statistic which is highly desirable but which we have been unable to achieve. One would like to be able to evaluate the *absolute* statistical significance of any filamentary structure detected, namely the probability that it would occur by chance in *any* distribution without a real tendency to linear connectedness. In practice we have only been able to compute the probability of chance occurrence in *particular* sorts of nonfilamentary distributions by explicit comparison.

This difficulty will strongly limit the generality of our conclusions and stands as a challenge to future work.

b) Procedure

The algorithm is designed to pick out the ridges and peaks in a two-dimensional data set. It does this locally by examining each pixel and its eight nearest neighbors as follows. Consider each of the four axes defined by pixel i and its eight nearest neighbors (see Fig. 2). Examine each axis to determine whether pixel i is a local maximum along that axis. Pixel i is a directional maximum along an axis if the number of galaxies in pixel i is greater than or equal to the number of galaxies in both neighboring pixels on that axis. Let D^i be the number of directional maxima for pixel i. Pixel i is called a peak pixel if $D^i = 4$, a ridge pixel if $D^i = 2$ or 3, and a background pixel if $D^i = 0$ or 1. Filaments are defined to consist of contiguous sets of ridge and peak pixels.

Essentially all algorithms which we have been able to invent require at least one parameter to determine the resolution with which one examines the data. For the above algorithm this is the pixel size, which is important because the algorithm is best able to pick out filaments whose width is on the order of the pixel size. In addition the data's smoothness is important because excessive counting noise on the scale of a single pixel will prevent the algorithm, which works locally, from detecting large-scale structure. If the data are not of sufficient signal-to-noise ratio, small-scale smoothing must be introduced.

III. APPLICATION

a) Data and Controls

We have applied our mapping technique to the Shane-Wirtanen distribution, the Soneira and Peebles (1978) model universe, and to a randomly scrambled version
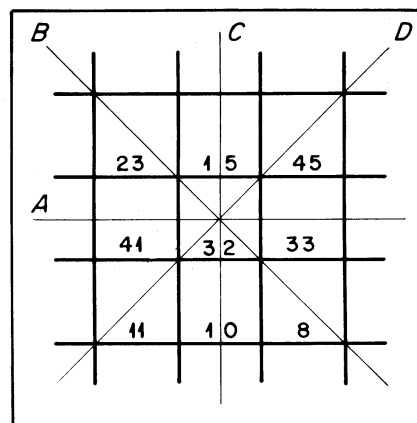

FIG. 2.—The definition of filament pixels. A pixel is classified by considering the galaxy count in it and its eight adjoining neighbors; a typical possible set of data is shown by the numbers. The D value of the pixel is defined to be the number of the four axes A, B, C, and D on which the (central) pixel galaxy count is larger than that of both of its neighbors on that axis. In the example $D = 2$ since this condition is satisfied for axes B and C but not A and D. All pixels with $D > 1$ are classified as filament pixels.

of the Shane-Wirtanen map. The model universe and scrambled map serve as our controls.

The real galaxy counts were mapped and provided by Mike Seldner. This reduction of the Lick catalog (Seldner *et al.* 1977) is a polar coordinate projection of the Northern Galactic Hemisphere where the galactic north pole serves as the origin of the coordinate system and radius is proportional to galactic colatitude. Each pixel is roughly 10′ across. We restricted our analysis to the 512×512 region of 10′ pixels centered on the galactic north pole and bounded at the edge by $b = 40°$.

The model universe was provided by Ray Soneira. This particular model is the final, published model of a whole series of computer simulations; it not only has the correct two-, three-, and four-point correlation functions, but it is the one which Soneira and Peebles feel most closely mimics the overall appearance of the data. The model map also has roughly 10′ resolution, but differs from the real sample in that it is an equal area projection. When restricted to the same 512×512 pixel region with $b \geq 40$, however, the two projections are almost identical; the model has only slightly more pixels.

The scrambled map was produced by assigning the galaxy counts in each Shane-Wirtanen $10′ \times 10′$ bin to a new randomly chosen bin location in the sky.

b) Mapping

Our approach to mapping the filaments was to first work with the Shane-Wirtanen data alone until we had generated a good map; only then did we compare to the controls.

Our first application of the filament mapping algorithm was to the full resolution data. The results were not good. Only a few filaments detected by the eye were mapped; even worse, many structures not detected by the eye as filaments were mapped. It appeared that small-scale noise was dominating the filament maps. Thus, it was necessary to analyze a lower resolution picture. In particular, we used a 4×4 repixeling (Fig. 3 [Plate 2]) and smoothed the data by convolution with a gaussian of radius 2 40′ pixels. The effect of the repixeling and smoothing is shown in Figure 4 (Plate 3); superposed in white are the filaments detected by our algorithm. Figure 5 (Plate 4) shows the detected filaments with the background removed.

Based upon a detailed comparison of the filament map to the raw image, we contend that the algorithm has identified all of, and essentially only, those structures which have the visual appearance of filaments in the Shane-Wirtanen map.

However, the algorithm provides only approximate identification of filaments. A different 40′ pixeling or a slightly different smoothing radius would sever some of the long filaments and join some adjacent short filaments to make long ones. This ambiguity cannot be circumvented. With this defect in mind, we have purposely not tried to "fine-tune" the maps we present here; rather, we have simply used the most convenient 40′ pixeling and a "round number" smoothing radius.

c) Filament Width and Length

Filament maps were also generated with 10′, 20′, 80′, and 160′ pixeling, but none of these reproduced the visually striking features nearly so well as the 40′ pixeling. The 10′ and 20′ pixel maps were dominated by counting noise so that the value of D^i was not reliably determined for most pixels. The 80′ and 160′ maps produced only a few dense clusters marked as peaks by the algorithm. No large-scale filamentary or connecting structures were mapped. This suggests that the filaments may have a characteristic width in the 30′–60′ range, corresponding roughly to 3 h^{-1} to 5 h^{-1} Mpc at the mean depth of the catalog. Furthermore, since the typical scale of the most striking filaments is 10° (50 h^{-1} Mpc) and since we have observed no significant structures on any other scale, it seems that this may be a characteristic length scale for large-scale structure. If one imagines the universe as a "cosmic cobweb," this scale represents not only the typical length of filaments but also perhaps the characteristic diameter of voids and separation of large clusters.

d) Comparison to Model

The filament map which we have produced for the SW data bears a striking resemblance to the filaments which the eye sees in the data. However, the situation is less reassuring when the model's filament map is considered. Its appearance is quite similar to that of the data filament map, probably more similar than the raw images themselves! The filaments in the model map can be located in its raw image, but they are much less striking than those in the data. In comparing Figures 3 and 4, it appears that the smoothed maps are more similar than their raw parents. This is expected, because both raw distributions have the same intrinsic two-point correlation functions, and both have received the same artificial correlation, the two 40′ pixel smoothing. In view of the resulting visual similarity between the data and model filament maps, we now present a statistical comparison which considers pixel type, filament length and filament brightness.

Table 1 lists the total number and fractions of each pixel type (D value) for both samples. The similarity between the fractions of types 2, 3, and 4 is striking. In both model and real data, approximately 12% of the pixels and about 18% of the galaxies are in filaments. The greatest difference between the two samples appears in the background pixels, types 0 and 1. The fractions of pixel types, however, is to some extent a local effect, because it is not sensitive to how the pixels fit together to make a map. Since both maps resulted from the same small-scale smoothing, one might *not* expect large differences from two raw distributions with the same intrinsic correlation functions.

The distribution of filament lengths is a more telling global measure. Here we define length to be the distance along a filament between the two most widely separated pixels on the filament, and distance is the minimum number of 1 pixel steps, including diagonal ones, in a

TABLE 1

DISTRIBUTION OF PIXEL TYPES

| | SHANE-WIRTANEN | | MODEL | | SCRAMBLED | |
D VALUE	Number	Fraction	Number	Fraction	Model	Fraction
0.................	7347	0.527	7309	0.509	7713	0.553
1.................	4120	0.296	4465	0.311	3735	0.268
2.................	1544	0.111	1580	0.110	1611	0.116
3.................	525	0.038	571	0.040	567	0.041
4.................	396	0.028	426	0.030	315	0.023

path along the filament between the two pixels. This definition does not count in any way dead-end branches or redundant paths and is very conservative in that sense. The average angular distance in a 1 pixel step is about 48′. Table 2 gives the distribution of filament lengths for the model and the data filament maps. Again the similarities are striking: The Shane-Wirtanen map shows 296 filaments with a mean length of 3°45, while the model contains 322 filaments with a mean length of 3°31. Both have median filament lengths of about 2°. A Kolmogorov-Smirnov comparison of the two distributions shows no significant difference.

Despite these similarities, inspection of Table 2 does reveal one intriguing difference. The real data map contains substantially more very long filaments than the model map even though it contains slightly fewer total filaments. In particular, there are 17 filaments with lengths greater than 10° (=3 times the mean) in the real data map as compared to seven in the model. The a priori probability of such an asymmetry is fairly low (approximately 3.2%), but of course it was not predicted a priori but noticed a posteriori. Significant or not, it may explain in part the substantially more

filamentary appearance of the data as compared to the model.

Another factor which could easily affect the relative appearance of filaments in the model and data is the brightness (=galaxy count) contrast with which they appear. Here again there is a difference which favors filament visibility in the data. Figure 6 is a plot of the difference between the percentage of Shane-Wirtanen and model pixels with various galaxy densities for both the whole maps and for the filaments alone. The differences are small and not necessarily statistically significant but do indicate that the Shane-Wirtanen filaments are both relatively and absolutely bright compared to the model filaments.

These differences in filament length and contrast are statistically independent but may be related; there is some evidence that the same specific structures are responsible for both effects. This is seen by applying the following combined length and contrast criterion: A filament is "significant" if it has length greater than twice the mean and contains at least 1 pixel in the

TABLE 2

DISTRIBUTION OF FILAMENT LENGTHS

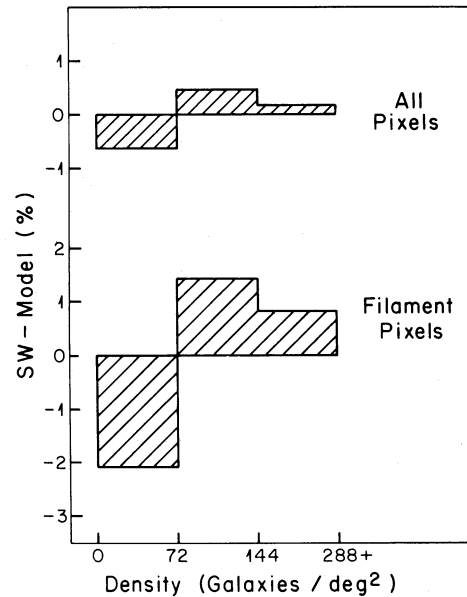| LENGTH | | | | |
Pixels	Degrees	SHANE-WIRTANEN	MODEL	SCRAMBLED
1	0.8	82	84	75
2	1.6	40	30	38
3	2.4	44	65	47
4	3.2	24	35	44
5	4.0	23	26	17
6	4.8	21	21	20
7	5.6	19	16	20
8	6.4	13	12	14
9	7.2	8	9	15
10	8.0	1	5	6
11	8.8	2	8	7
12	9.6	2	4	5
13	10.4	4	1	4
14	11.2	4	2	4
15	12.0	1	2	2
16	12.8	0	0	0
17	13.6	4	1	2
18	14.4	1	0	0
19	15.2	1	0	3
20	16.0	1	0	2
>20	>16.0	1 (27)	1 (25)	8

FIG. 6.—The difference in the percentage of Shane-Wirtanen data map pixels and Soneira-Peebles model map pixels with counts in each of three broad logarithmic bins. The data show that the SW map has more contrast than the model map and that this tendency is concentrated in the $D > 1$ filament pixels.

smoothed map with density $> = 72$ galaxies deg^{-2}. We use the smoothed galaxy counts to ensure that the filament passes through a high density region; the raw counts contain large fluctuations from pixel to pixel and are unsuitable for this purpose. We have chosen the 72 galaxies deg^{-2} requirement, because it corresponds to the typical smoothed density of the most noticeable filaments. Incidentally, 72 galaxies deg^{-2} corresponds to 2 galaxies per 10' pixel in the full-resolution data.

Application of this combined length and contrast criterion to our two cases shows a significant difference between the data and model; 16 data filaments passed the test, whereas only seven model filaments passed. This asymmetry represents an *a priori* probability of only 4.7%. Figure 7 shows the filaments which pass this criterion. The next section presents the SW filaments passing this criterion as a catalog.

An attempt to evaluate the meaning of the above statistical comparison is given in § V.

e) Comparison to Scrambled Map

Application of our algorithm to the map produced by scrambling the SW map also identified "filamentary" structures. Tables 1 and 2 give the data from a particular scrambled map analysis. Although the distributions of pixel D values and filament lengths are similar to those for the SW data and model, the scrambled map has a very different appearance due to the destruction of the galaxy clustering by scrambling and smoothing. Quantitatively, the number of pixels with density ≥ 72 galaxies deg^{-2} is reduced by a factor of $\gtrsim 100$ as is the probability that any particular long filament will contain one. The result is that most scrambled maps contain no "significant" filaments, and that the filaments identified by our algorithm are not visually impressive in these maps. Identification of a filament by the algorithm is apparently a necessary, but not a sufficient, condition for its visual detection.

IV. FILAMENT CATALOG

As we shall argue in § V, it is possible that the longest and/or brightest filaments in the Shane-Wirtanen galaxy counts are "real" structures in the sky. If so they certainly warrant observational study, and for this purpose, we map in Figure 7 the "significant" filaments (i.e., lengths $>7°2$ [twice the mean] and at least one pixel in the smoothed map with a galaxy density ≥ 72 deg^{-2}). In addition, Table 3 gives the center positions for the 40' × 40' pixels in six of these filaments. Note again that the mapping algorithm is only approximate and that this catalog therefore cannot be interpreted too rigorously.

V. DISCUSSION

Our results may be summarized as follows: A simple and objective algorithm which accurately identifies the filamentary structures in the Shane-Wirtanen galaxy count catalog has been defined; it also finds a set of visually less impressive filaments in a static hierarchical model of the clustering constructed by Soneira and

Peebles (1978) which has no inherent filamentary nature. The statistical properties of the filaments in the model are quite similar to those in the data, but there is a significant excess of long and bright filaments in the data relative to the model. There are at least two different possible interpretations of these facts.

One possible view is that the statistical tests, length or length plus contrast, which indicates more filamentary structure in the data than in the model at better than 95% confidence, constitute a fair case for believing the filaments to be "real" and thus not statistical fluctuations or optical illusions. The considerable simularity between the model and the data filaments could be attributed to the fact that in both cases the vast majority of the filaments are quite short and may simply be a product of their identical intrinsic auto-correlation functions and the smoothing applied to both maps. The true signal may be entirely carried by long and high contrast linear features which are present in the Shane-Wirtanen map but not in the Soneira-Peebles model. Indeed, it might be argued that this model is a very conservative comparator for the data, since there was much freedom in how it was constructed and wide experimentation was employed to get a map which "looked" as much like the Shane-Wirtanen map as possible, including explicitly its filamentary appearance. There is no reason to suppose that a generic hierarchical clustering model or an N-body calculation could produce so many filaments as the static simulation we have analyzed. In addition, our mapping method requires the introduction of smoothing; this tends to

TABLE 3
FILAMENT CATALOG

b	l	$\alpha(1950)$			$\delta(1950)$
		Filament 1			
55.38	8.97	4^h 6^m		1^s	9°59'
55.48	7.79	4 4		7	9 29
56.19	7.96	4 2		8	9 59
57.00	6.89	4 8		5	9 58
57.72	7.05	4 5		6	10 28
58.43	7.21	4 3		6	10 57
58.33	8.50	4 5		1	11 27
59.04	8.70	4 3		1	11 56
59.64	10.24	4 3		7	12 55
60.34	10.49	4 1		7	13 34
60.20	11.85	4 3		4	13 54
60.91	12.14	4 0		3	14 23
61.61	12.45	4 8		2	14 52
62.32	12.77	4 6		1	15 22
60.75	13.52	4 2		2	14 53
61.27	15.26	4 2		2	15 52
61.07	16.63	4 4		3	16 22
60.86	17.99	4 6		5	16 51
60.63	19.32	4 8		9	17 20
60.38	20.64	4 0		4	17 50
61.05	21.14	4 8		4	18 19
60.78	22.46	4 0		0	18 48
60.50	23.75	4 2		8	19 17
60.86	25.62	4 2		7	20 16

TABLE 3—*Continued*

b	l	α(1950)			δ(1950)	
		Filament 2				
58.88	29.83	5	3	3	21	38
59.23	28.66	5	1	0	21	10
59.86	29.32	4	9	2	21	41
60.20	28.11	4	7	9	21	13
60.84	28.78	4	5	0	21	43
61.47	29.48	4	2	0	22	13
61.81	28.20	4	0	7	21	45
62.45	28.91	4	8	7	22	15
63.07	29.65	4	6	5	22	45
64.06	29.05	4	2	1	22	46
64.68	29.85	4	9	8	23	16
65.30	30.68	4	7	3	23	46
65.92	31.55	4	5	9	24	16
65.66	29.22	4	5	2	23	17
66.29	30.07	4	3	7	23	46
66.91	30.96	4	0	1	24	16
67.52	31.91	4	8	4	24	45
67.73	34.46	4	8	9	25	45
68.32	35.54	4	6	1	26	15
68.90	36.67	4	3	2	26	44
69.91	36.25	4	9	8	26	43
70.92	35.79	4	4	5	26	41
71.50	37.09	4	2	2	27	10
71.92	35.27	4	0	2	26	38
72.33	33.37	4	8	3	26	7
72.50	36.63	4	7	8	27	7
72.92	34.70	4	5	9	26	35
73.51	36.12	4	3	4	27	4
74.09	37.65	4	0	8	27	32
74.65	39.29	3	8	1	28	0
75.20	41.05	3	5	3	28	28
75.66	38.88	3	3	5	27	56
76.22	40.76	3	1	6	28	24
76.68	38.42	3	9	0	27	51
77.11	35.91	3	7	5	27	18
76.29	29.93	3	9	8	25	50
76.91	31.50	3	7	0	26	18
77.52	33.23	3	5	1	26	45
78.11	35.13	3	2	1	27	12
79.12	34.22	3	7	8	27	6
		Filament 4				
73.93	106.82	3	3	7	42	48
73.14	106.11	3	5	8	43	23
72.92	108.43	3	2	0	43	48
72.68	110.70	3	9	9	44	14
71.75	112.01	3	8	7	45	14
71.08	111.19	3	0	1	45	49
70.81	113.20	3	7	4	46	14
70.14	112.38	3	9	0	46	49
69.20	113.46	3	9	7	47	50
68.25	114.44	3	8	3	48	50
67.94	116.15	3	4	5	49	15
66.98	116.97	3	3	5	50	15
66.64	118.54	3	0	9	50	40
66.01	117.72	3	2	3	51	15
65.66	119.22	2	9	3	51	40
65.03	118.41	3	1	9	52	15

b	l	α(1950)			δ(1950)	
		Filament 10				
42.34	248.28	10	20	7	− 3	57
42.06	247.48	10	17	42	− 3	42
42.73	247.15	10	18	59	− 3	4
42.44	246.35	10	16	33	− 2	49
42.81	245.19	10	15	23	− 1	57
42.50	244.41	10	12	56	− 1	43
43.15	244.03	10	14	10	− 1	5
42.83	243.24	10	11	43	− 0	51
42.50	242.46	10	9	15	− 0	37
43.14	242.06	10	10	28	− 0	0
42.16	241.70	10	6	46	− 0	23
41.82	240.95	10	4	18	− 0	10
		Filament 12				
45.66	259.24	10	52	27	− 6	49
46.37	259.06	10	53	50	− 6	11
46.50	259.99	10	56	12	− 6	29
47.21	259.82	10	57	34	− 5	51
47.33	260.78	10	59	56	− 6	8
48.04	260.62	11	1	18	− 5	31
48.15	261.59	11	3	40	− 5	48
48.86	261.44	11	5	3	− 5	10
48.96	262.44	11	7	25	− 5	29
49.68	262.30	11	8	47	− 4	51
50.39	262.16	11	10	10	− 4	13
50.48	263.20	11	12	32	− 4	31
51.20	263.07	11	13	54	− 3	53
51.28	264.13	11	16	17	− 4	11
51.34	265.19	11	18	39	− 4	30
52.12	266.19	11	22	24	− 4	11
52.16	267.27	11	24	46	− 4	30
52.18	268.36	11	27	7	− 4	49
52.90	268.33	11	28	31	− 4	11
53.62	268.30	11	29	54	− 3	34
54.34	268.26	11	31	18	− 2	56
54.36	269.42	11	33	40	− 3	15
		Filament 13				
49.24	317.15	13	26	36	− 12	18
48.71	317.83	13	28	53	− 12	43
48.17	318.49	13	31	9	− 13	8
49.19	318.58	13	30	22	− 12	8
49.66	319.34	13	31	51	− 11	33
49.57	320.78	13	35	37	− 11	24
49.46	322.21	13	39	24	− 11	14
49.90	323.03	13	40	54	− 10	40
49.32	323.64	13	43	10	− 11	5
48.74	324.23	13	45	26	− 11	31
48.15	324.81	13	47	42	− 11	56
47.56	325.37	13	49	58	− 12	22
47.96	326.17	13	51	28	− 11	48
48.36	327.00	13	52	58	− 11	14
48.14	328.36	13	56	44	− 11	5
48.51	329.21	13	58	15	− 10	32
47.89	329.71	14	0	31	− 10	58
48.25	330.56	14	2	2	− 10	24
48.60	331.43	14	3	33	− 9	50
49.57	331.84	14	2	49	− 8	51
49.91	332.74	14	4	21	− 8	17
50.23	333.67	14	5	54	− 7	44
50.55	334.60	14	7	27	− 7	10

MODEL
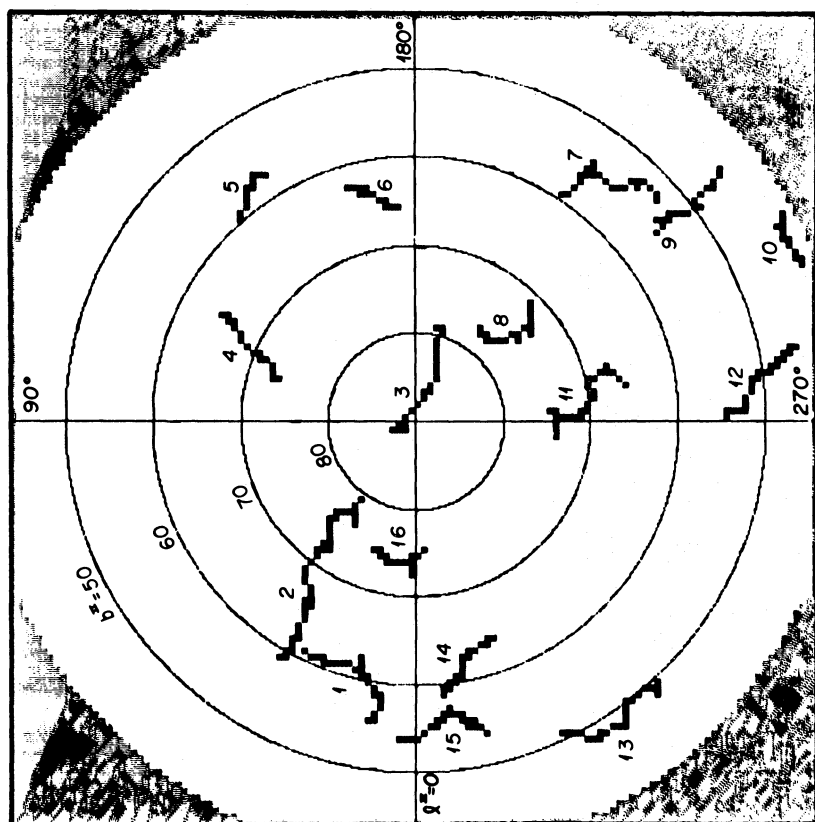
SW

Fig. 7.—Significant filament maps. Only those filaments with lengths greater than twice the mean and at least one pixel with greater than 72 galaxies per square degree in the smoothed map are shown. The Fig. 1 coordinate system is again used, but no gray scale is employed. These long bright filaments which are substantially more common in the SW data than they are in the Soneira-Peebles model account for the former's more filamentary appearance.
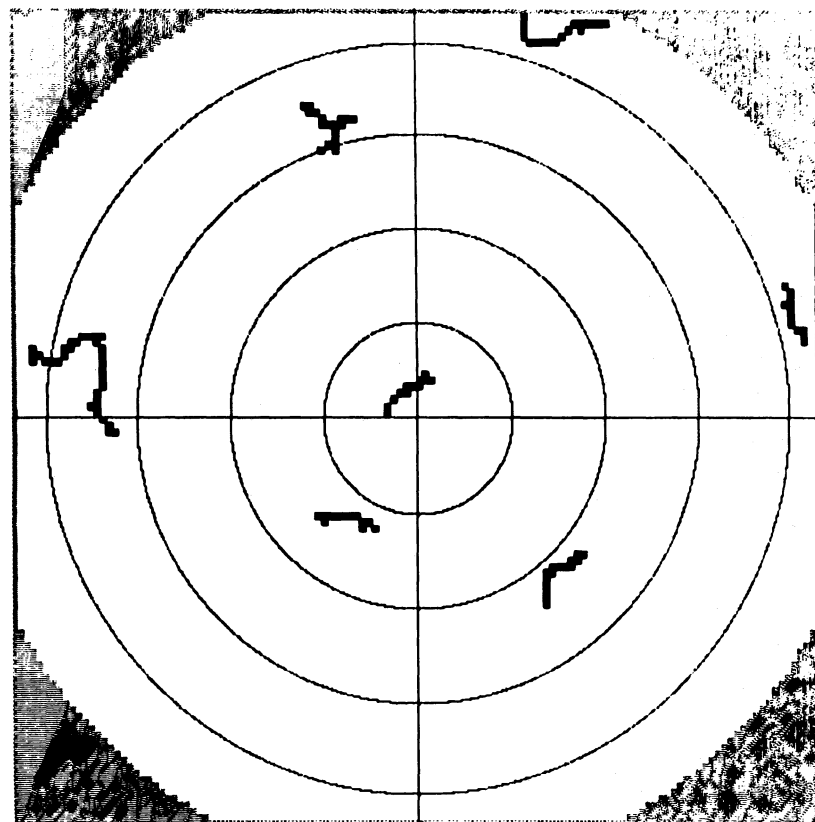
make dissimilar data more similar. It can therefore be argued that any differences detected between the data and model are actually indicative of greater differences in the raw images.

A second and more skeptical view of our results is that they greatly weaken the visual evidence for filaments in the Shane-Wirtanen catalog. No very great differences between the data and the Soneira-Peebles model were uncovered and those that were found can be explained away as the results of *a posteriori* statistics. This argument can be spelled out more fully as follows: A peculiar feature of the visual appearance of the data maps was noticed, and then great effort was expended to devise a statistic (=mapping algorithm) maximally sensitive to just the features which had been observed. Nevertheless, application of this procedure to both the model and the data demonstrated that even in this highly specific way they are strikingly similar. Close inspection of filament properties in the two maps did yield a 2 σ difference which may explain why the eye is more struck by the data than by the model filaments but which does not demonstrate any fundamental difference between the two distributions. Finally, it should be understood that even if the particular Soneira-Peebles model analyzed here cannot explain every feature of the Shane-Wirtanen map, it does *not* follow that all simple hierarchical clustering models would fail to do so.

We do not believe that there is currently sufficient information to decisively choose between the two alternatives described above. Nevertheless, we do feel that the issue can be resolved either through future observational work or by further statistical analyses.

REFERENCES

Bond, J. R., Efstathiou, G., and Silk, J. 1980, *Phys. Rev. Letters*, **45**, 1980.
Chincarini, G. 1978, *Nature*, **272**, 515.
Davis, M., Huchra, J., Latham, D. W., and Tonry, J. 1982, *Ap. J.*, **253**, 423.
Doroshkevich, A. G., Kotok, M. Y., Novikov, I. D., Polyndov, A. N., Shandarian, S. F., and Sigov, Yu. S. 1980, *M.N.R.A.S.*, **192**, 321.
Einasto, J., Joveer, M., and Saar, E. 1980, *M.N.R.A.S.*, **193**, 353.
Fry, J. N., and Peebles, P. J. E. 1978, *Ap. J.*, **221**, 19.
Gregory, S. A., Thompson, L. A., and Tifft, W. G. 1981, *Ap. J.*, **243**, 411.
Ikeuchi, S. 1981, *Pub. Astron. Soc. Japan*, **33**, 211.
Joveer, M., Einasto, J., and Tago, E. 1978, *M.N.R.A.S.*, **185**, 357.
Kuhn, J. R., and Uson, J. M. 1982, *Ap. J. (Letters)*, **263**, L47.
Ostriker, J. P., and Cowie, L. L. 1981, *Ap. J. (Letters)*, **243**, L127.

Peebles, P. J. E., and Groth, E. J. 1975, *Ap. J.*, **196**, 1.
Seldner, M., Siebers, B., Groth, E. J., and Peebles, P. J. E. 1977, *A.J.*, **82**, 249.
Seldner, M., and Uson, J. M. 1983, *Ap. J.*, **264**, 1.
Soneira, R. M., and Peebles, P. J. E. 1978, *A.J.*, **83**, 845.
Sunyaev, R. A., and Zel'dovich, Ya. B. 1972, *Astr. Ap.*, **20**, 189.
Tarenghi, M., Chincarini, G., Rood, H. J., and Thompson, L. A. 1980, *Ap. J.*, **235**, 724.
Tarenghi, M., Tifft, W. G., Chincarini, G., Rood, H. J., and Thompson, L. A. 1979, *Ap. J.*, **234**, 793.
Tully, R. B. 1982, *Ap. J.*, **257**, 389.
Zel'dovich, Ya. B. 1970, *Astr. Ap.*, **5**, 84.
Zel'dovich, Ya. B., Einasto, J., and Shandarian, S. F. 1982, preprint.

J. R. GOTT and E. L. TURNER: Princeton University Observatory, Peyton Hall, Princeton, NJ   08544

J. E. MOODY: Institute for Theoretical Physics, UCSB, Santa Barbara, CA   93106

PLATE 1

SW
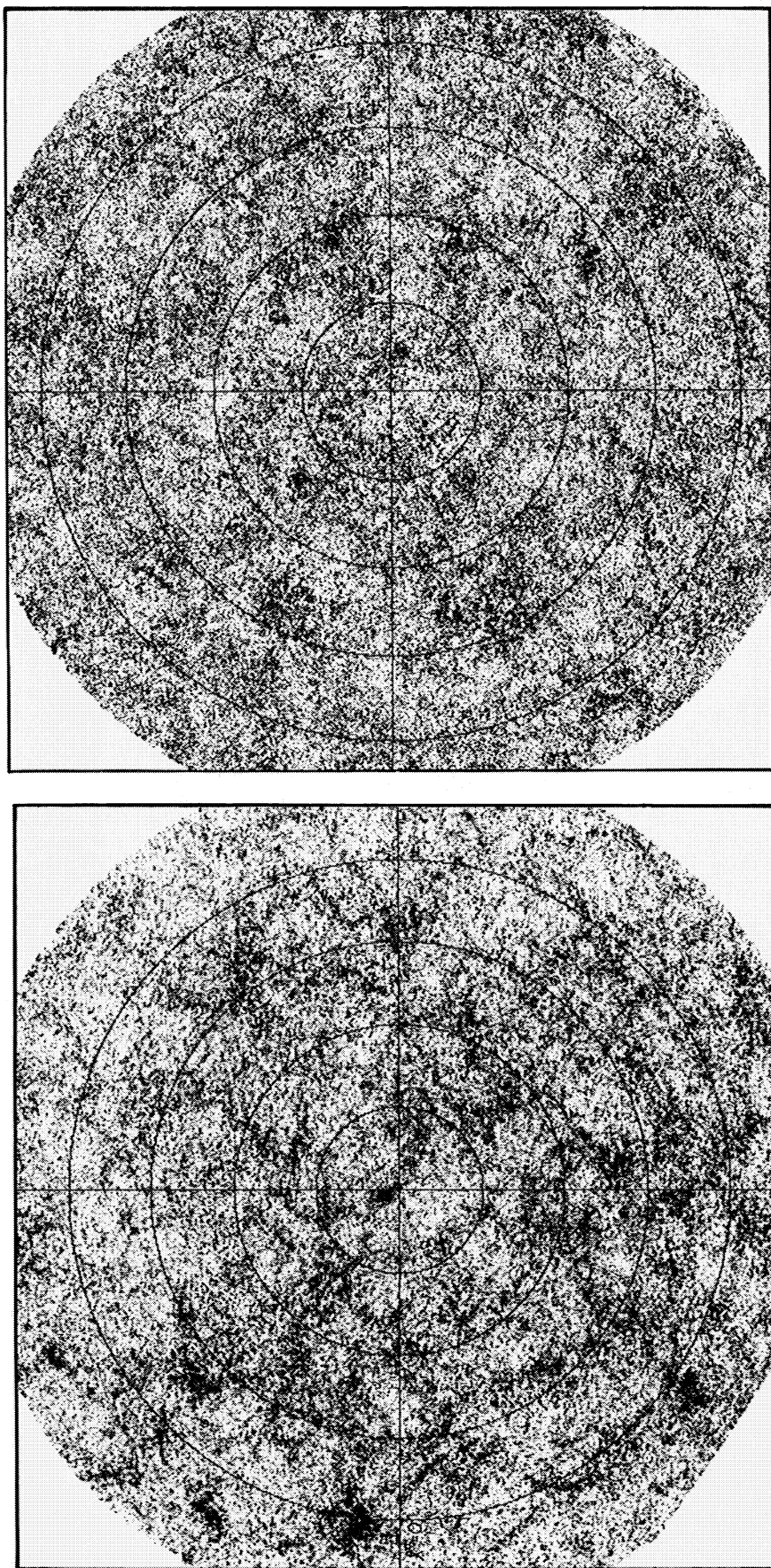
MODEL

FIG. 1.—The Shane-Wirtanen galaxy count catalog map and the Soniera-Peebles hierarchical clustering model computer simulation of it. The maps have a 10' × 10' resolution and show the region of sky which we have analyzed for filamentary structure. The gray scale shows regions of greater galaxy counts as darker and has a smaller dynamic range than the one employed by Soneira and Peebles (1978). The coordinate system is centered on the North Galactic Pole with the $l = 0$ line at 9 o'clock (longitude increasing clockwise) and circles of galactic latitude at 10° intervals.

MOODY *et al.* (*see* page 16)

PLATE 2

MODEL

SW

≤ 8 9-12 13-16 17-20 21-24 25-28 29-32 33-36 37 ≤
GALAXIES PER PIXEL

≤18 19-27 28-36 37-45 46-54 55-63 64-72 73-81 82 ≤
GALAXIES PER □°
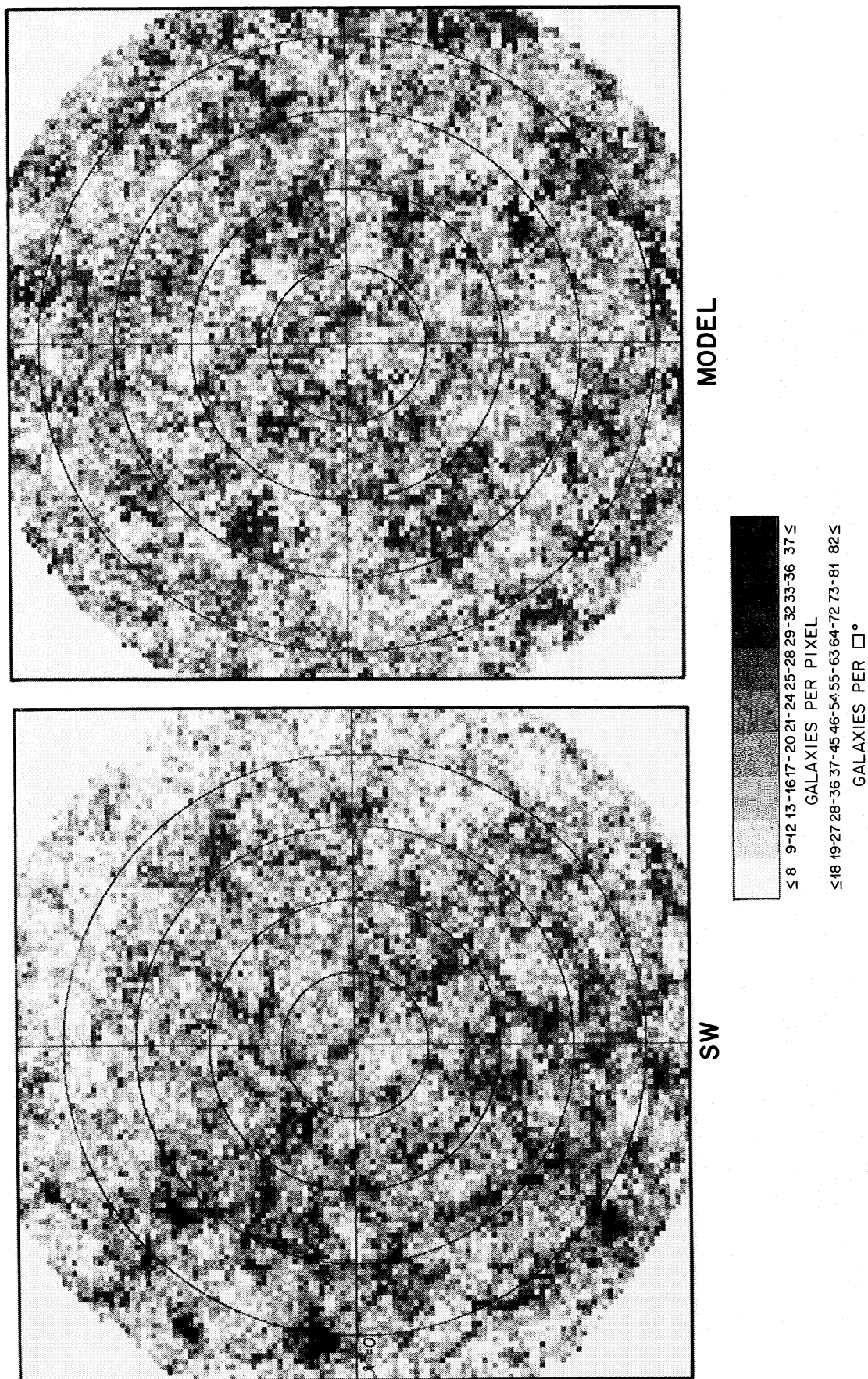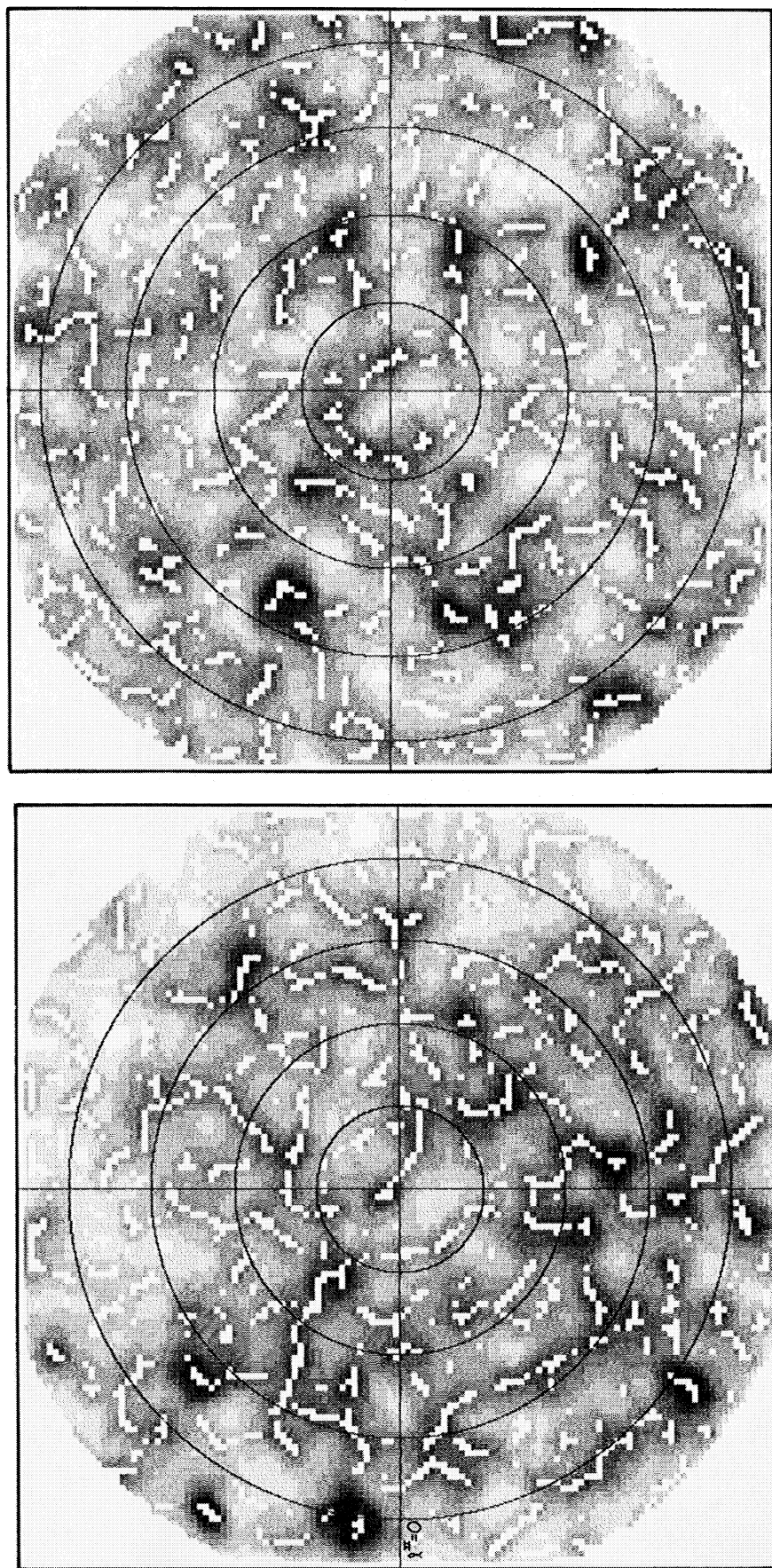
Fig. 3.—Low-resolution (40' × 40') maps of the SW data and the computer model. The coordinate system is as in Fig. 1. The gray scale key is given both in galaxies per pixel and in galaxies per square degree. Large-scale structure in these maps may be best seen by viewing them from a distance.

Moody et al. (see page 18)
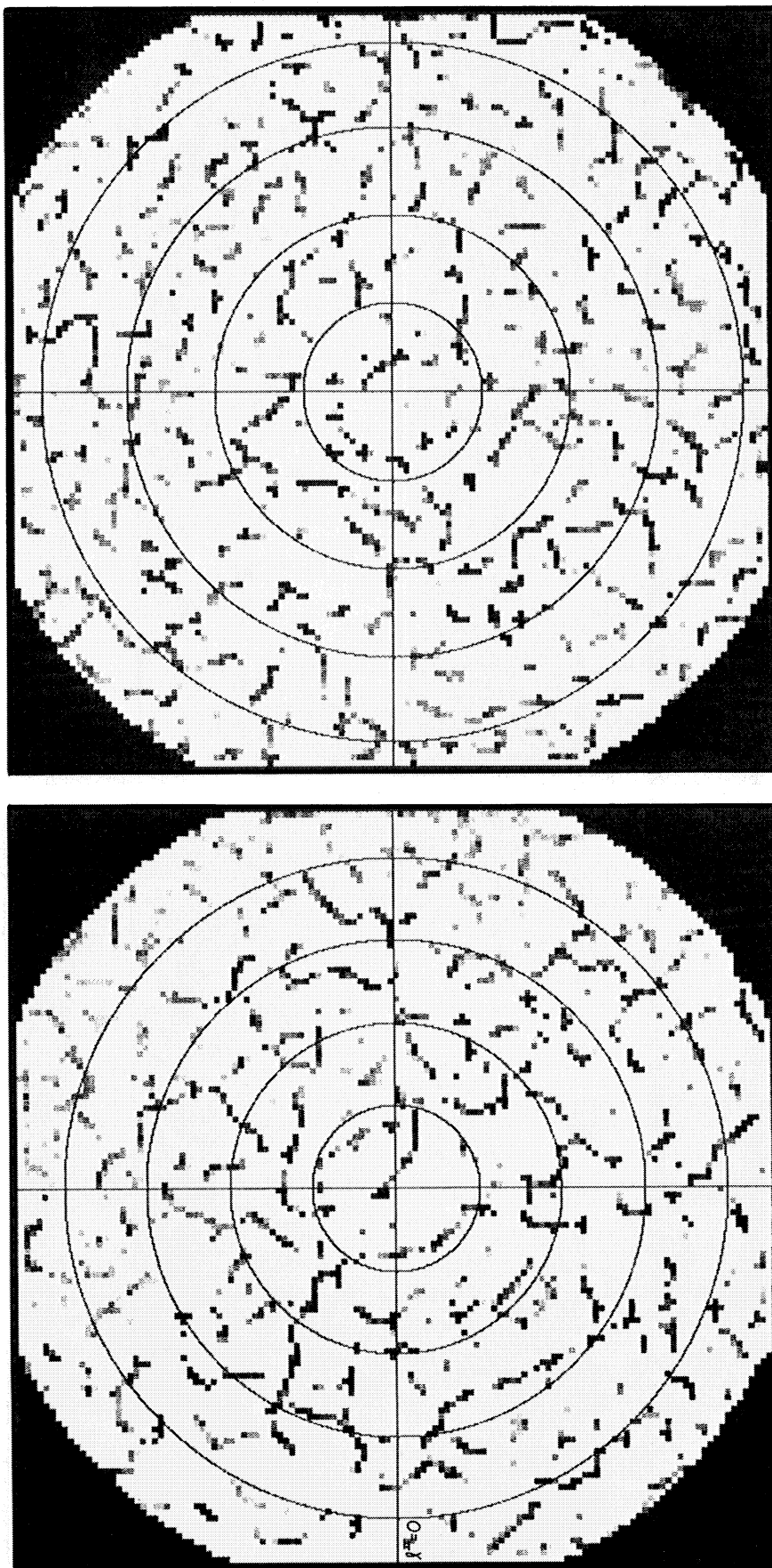
PLATE 3

MODEL

SW

Fig. 4.—Smoothed maps with filaments superposed. Using the same coordinate system as Fig. 1 and the Fig. 3 gray scale, the result of smoothing the low-resolution maps with a Gaussian of 2 pixels radius, applying our filament algorithm, and setting the $D > 1$ filaments to 0 counts is shown.

MOODY et al. (see page 18)

PLATE 4

MODEL

SW

Fig. 5.—Filament maps with background removed. All $40' \times 40'$ pixels with $D > 1$ are plotted using the Fig. 3 gray scale and their unsmoothed counts on the Fig. 1 coordinate system while all $D < 2$ pixels are set to 0.

Moody et al. (see page 18)